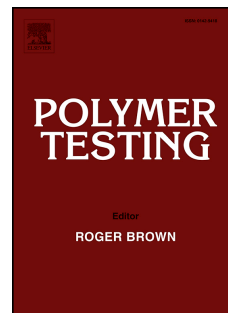# Accepted Manuscript

Nanocomposites with shape memory behavior based on a segmented polyurethane and magnetic nanostructures

G.D. Soto, C. Meiorin, D. Actis, P. Mendoza Zélis, M.A. Mosiewicki, N.E. Marcovich

Please cite this article as: G.D. Soto, C. Meiorin, D. Actis, P. Mendoza Zélis, M.A. Mosiewicki, N.E. Marcovich, Nanocomposites with shape memory behavior based on a segmented polyurethane and magnetic nanostructures, *Polymer Testing* (2018), doi: 10.1016/j.polymertesting.2017.12.012.

Material Behaviour

NANOCOMPOSITES WITH SHAPE MEMORY BEHAVIOR BASED ON A SEGMENTED POLYURETHANE AND MAGNETIC NANOSTRUCTURES

G. D. Soto[1], C. Meiorin[1], D. Actis[2], P. Mendoza Zélis[2], M. A. Mosiewicki[1], N. E. Marcovich[1]*

[1] Instituto de Investigaciones en Ciencia y Tecnología de Materiales (INTEMA-CONICET)
Juan B. Justo 4302, Mar del Plata, Buenos Aires, Argentina; CP 7600
[2] Instituto de Física La Plata (CONICET), Universidad Nacional de La Plata;
Calle 49 y 115, La Plata, Buenos Aires, Argentina; CP 1900

ABSTRACT

Shape-memory composites based on a commercial segmented polyurethane and magnetite (Fe_3O_4) nanoparticles (NPs) were prepared by a simple suspension casting method. The properties of the resulting nanocomposites, containing 1 to 10 nominal wt.% magnetic particles, were evaluated by thermogravimetric tests, contact angle measurements, differential scanning calorimetry, infrared and X-ray spectroscopy, static and thermal cyclic tensile tests, dynamic mechanical analysis and experiments of alternating-magnetic-field heating. It was found that most of the suspended NPs could be successfully incorporated into the polyurethane matrix, and thus composite samples with up to 7 wt.% actual concentration were obtained. On the other hand, the incorporation of magnetite nanoparticles to the shape memory polyurethane did not significantly affect most of the matrix properties, including its shape memory behavior, while added magnetic response to the nanocomposites. Thus, nanocomposites were able to increase in temperature when exposed to an alternating magnetic field, which allowed them to recover their original shape quickly by an indirect triggering method.

KEYWORDS: polymeric nanocomposites; shape memory behavior; magnetic nanostructures; indirect triggering method.

1. INTRODUCTION

Shape-memory polymers (SMP) have been an active area of intensive scientific research & development over the past 20 years. Their unusual properties find several novel and important uses, including in biomedical and aerospace fields. This particular class of materials has the unique ability to keep transient shapes and recover their original ones by the application of an external stimulus such as temperature, pH, light, moisture, electric field, magnetic field, specific ions and enzymes [1-8]. In comparison with others shape-memory materials such as alloys (SMA) or ceramics, SMP offer several technological advantages because of their low density, good recoverability, ease of processing, low cost and tailoring of properties according to the desirable functionality [1, 2]. SMP are even more interesting because they are able to store and recover large strains in response to the stimulus [1, 9, 10]. Thus, in recent years, SMP have become among the main components of intelligent and smart devices [1-8].

Within the SMP field, segmented polyurethanes (SPU) are one of the most usual types. SPU are multiblock copolymers formed by hard and soft molecular segments. Due to structural differences, SPU are rarely in thermo-dynamical equilibrium and can separate in phases, arranging domains with different thermal and mechanical properties [11-13]. The hard segments in these PU multiblock copolymers that associate themselves through dipole-dipole interactions, hydrogen bonding or crystallization, are composed of alternating diisocyanate and short chain extender molecules. These hard segments have the ability to memorize the permanent shape, determining the shape retention. On the other hand, the soft segments mainly constituted by long chain diols, are responsible for the thermally reversible phase transformation, which allow recovering the original shape [10, 14].

In these polymers, the phase with the highest thermal transition temperature (Tperm) acts as net point, while the chain segments associated with the domains with the second highest thermal transition temperature (Ttrans) are called switching segments. Thus, switching segments are flexible if the working temperature is higher than Ttrans: if a sample is deformed by the application of an external stress, it returns to its original shape once the external stress is released [15]. Ideal shape memory behavior requires a sharp transition

from glassy state to rubbery state, a long relaxation time and high ratio of glassy to rubbery modulus [15].

The interest behind developing SPU lies mainly in their simplicity of processing and low cost [1, 16]. However, one of the major drawbacks for certain applications is their low stiffness which results in a relatively weak recovery force after constraint [10, 12]. Different authors report enhancement in the mechanical properties after the addition of rigid fillers such as fibers or particles to SMP matrices [1-6]. Auad and col. [10, 12], for example, dispersed uniformly a small amount of nanocelullose (up to 1%) in segmented polyurethane matrices, increasing the modulus without altering the shape memory behavior of the resulting composite with respect to that of the neat PU matrix. In this regard, one attractive alternative to study is the incorporation of magnetite nanoparticles (NPs) to the SPU polymeric network, not only to improve the recovery force, but also to modify their structure, leading to the incorporation of interesting functional properties. Among the advantages of a polymeric matrix embedded with NPs is the possibility to respond at a distance in different ways both to static as well as alternating magnetic fields. The static fields produce a net force on the material allowing movement, while the alternating fields generate a rapid and homogeneous heating effect without direct contact with a thermal source. In this method, the application of a radiofrequency field to a magnetic system would induce remarkable heating effects by the energy dissipated during rapid magnetization reversal [17].

NPs have been incorporated recently with success in different polymeric matrices leading to novel materials with potential applications in, for example, biomedicine, biotechnology and materials science [1-6, 18-22]. However, only a few works relate to the addition of magnetite NPs to a segmented polyurethane matrix and the effect of the nanoparticles on the structural and functional properties of the nanocomposites [23-26].

Thus, the aim of this work is to characterize shape-memory nanocomposites based on a segmented polyurethane polymeric matrix and magnetite nanoparticles. The relationship between thermal, mechanical and functional properties (shape-memory and magnetic properties) and concentration of nanoparticles is presented and discussed.

2. MATERIALS AND METHODS

2.1. Materials

PU-NPs composites were prepared using a high-performance polyester thermoplastic PU (IROGRAN PS455-203, Huntsman) as matrix. This linear segmented PU has a low glass transition temperature ($Tg = -46.5$ °C, determined by differential scanning calorimetry, DSC), near-ambient melting of soft-segment crystallites ($Tm,s = 39$ °C, determined by DSC), high deformation (*ca.* 460%, measured at a crosshead speed of 10 mm min^{-1}) and strain-induced crystallization.

The following chemical products (Aldrich) were used as received in the synthesis of the magnetic nanoparticles: ferric chloride hexahydrate ($FeCl_3 \cdot 6H_2O$), ferrous chloride tetrahydrate ($FeCl_2.4H_2O$), ammonium hydroxide (28-30% NH_3) and N,N-dimethylformamide (99.8%).

2.2. Preparation Methods

2.2.1. Synthesis of magnetic nanoparticles (NPs)

NPs were prepared following the co-precipitation method suggested by Massart and Cabuil [27] with some modifications to improve the yield. In brief, 0.09 mol of $FeCl_3 \cdot 6H_2O$ and 0.06 mol of $FeCl_2.4H_2O$ were poured into a flask containing 50 mL of distilled water and heated at 70ºC to dissolve the salts. Then, 40 mL of NH_4OH were added and the formation of a black precipitate was immediately observed. With the help of a super-magnet positioned out of the flask, the NPs were decanted and collected into centrifugation tubes. The obtained NPs were washed until neutral pH with distilled water, separating the water used in each wash by centrifugation. Finally, the NPs were placed in a Petri dish and lyophilized. The obtained dark thin powder was preserved in a reagent bottle.

2.2.2. Preparation of nanocomposites

PU pellets were dissolved in dimethylformamide (DMF) up to 20 wt.% at room temperature by using a magnetic stirrer, and then mixed with the previously synthesized NPs in suitable ratios to obtain composite samples containing 0, 1, 3, 5, 7 and 10 nominal wt. % of NPs. The mixture was then ultrasonicated for 6 hours to obtain a stable and homogeneous suspension. PU composites films (approximately 0.75 mm in thickness) were

prepared by solvent casting of the final suspensions on an glass plate followed by drying in a convection oven at 80ºC for 24 hours.

2.3. Characterization Techniques

2.3.1. Thermogravimetric analysis (TGA). The thermal decomposition curves were obtained using a TGA-50 SHIMADZU Thermogravimetric Analyzer at a heating rate of 10°C/min, from 40°C up to 800°C under air atmosphere. The initial degradation temperature (Ti) was arbitrarily taken as the temperature at which the sample lost 5% of the initial weight. The temperature at which the samples undergo the maximum degradation rate (Tm) was obtained from the derivative TGA curves.

2.3.2. Contact angle

The surface hydrophobicity of the films was estimated by the sessile drop method, based on optical contact angle measurement using a Ramé Hart goniometer. A droplet of ethylene–glycol (Aldrich Co.) (5 µL) was deposited on the film surface with an automatic piston syringe. The drop image was photographed using a digital camera immediately after the drop deposition. Image analyzer software was used to measure the angle formed between the surface of the film in contact with the drop, and the tangent to the drop of liquid at the point of contact with the film surface. Three measurements each minute were performed on both sides of the films at 24ºC ± 2ºC.

2.3.3. Differential Scanning Calorimetry (DSC)

Differential scanning calorimetry (DSC) testing of the samples was performed using a calorimeter (Perkin Elmer Pyris 1) equipped with a cooling unit, and operating under nitrogen atmosphere (20 ml/min). Measurements were performed at 5°C/min. The average values of at least three replicates of each sample were reported.

2.3.4. Infrared spectroscopy (FT-IR)

FT-IR spectra of the magnetite particles, neat PU and nanocomposites were recorded by the attenuated total reflection method (ATR) using a Thermo Scientific Nicolet 6700 FT-IR spectrometer. The spectra were registered over the range of 500-4000 cm^{-1} with a resolution of 2 cm^{-1} and averaged over 32 scans.

2.3.5. X-ray diffraction (XRD)

X-ray diffraction spectra of NPs, neat PU and nanocomposites were obtained with a PANalytical X'Pert Pro diffractometer using a Cu K radiation source (0.1546 nm) operating at 40 kV and 40 mA.

2.3.6. Static tensile tests

These tests were performed at room temperature on specimens of 5 mm x 35 mm x 0.8 mm, using a universal testing machine (INSTRON 8501), in accordance with ASTM D 1708-02a. A crosshead speed of 10 mm/min was used. Young's modulus (E), yield stress (σ_y) and elongation at break (ε_b) were determined from the average values of four replicates for each sample.

2.3.7. Dynamical-mechanical tests (DMA)

The dynamic mechanical response of the samples was evaluated with an Anton Paar Physica MCR rheometer. Torsion geometry was used with bar specimens of ~35 mm x 5 mm x 0.8 mm. Measurements were performed as temperature sweeps in the range -70 to 55ºC at a heating rate of 5ºC/min. The frequency was kept at 1 Hz and the applied deformation at 0.1% to ensure working in the linear viscoelastic range. The Tg values were arbitrarily taken as the temperature at which a maximum in the tan δ curve was observed.

2.3.8. Thermal cyclic tests were performed on microtensile specimens of 5 mm x 25 mm x 8 mm using a universal testing machine equipped with a heating chamber (Instron 8501). Samples were first conditioned at 30 °C for 5 min and subsequently elongated to 100% of the original length at a speed of 5 mm min^{-1}. Then, the samples were cooled to -48 °C and unloaded. Finally, the samples underwent the recovery process by heating for 5 min at 30 °C. The strain maintained after unloading, and the residual strain of each cycle (N) were used to calculate the fixity (R_f) and recovery (R_r) ratios from these tests, as indicated in the following equations:

$$R_f(N) = \frac{\varepsilon_u}{\varepsilon_m} \times 100\% \qquad (1)$$

$$R_r(N) = \frac{\varepsilon_m - \varepsilon_p(N)}{\varepsilon_m - \varepsilon_p(N-1)} \times 100\% \qquad (2)$$

where ε_m is the maximum strain in the cycle (100%), ε_u is the residual strain after unloading at -48 °C, and ε_p is the residual strain after recovery.

2.3.9. Magnetic nanoparticle heating

The heating response of nanocomposites under an alternating magnetic field was characterized using inductive heating equipment (a power source-resonator set Hüttinger TIG 2,5/300) with an alternant field of 48 kA/m-and a frequency of 260 kHz. The nanocomposite temperature was measured by an optic fiber sensor (Neoptix T1) immersed in the center of the material and connected to an interface (Neoptix Reflex). Also, images taken with a thermographic camera TESTO 870-1 were recorded.

3. RESULTS AND DISCUSSION

3.1. Thermogravimetric analysis

Thermogravimetric analysis was used to study the thermal stability of the magnetic composites and also to check the concentration of magnetite nanoparticles effectively retained into the polyurethane matrix. The mass fraction of NPs in each sample was calculated from the corresponding char content, obtained as the mass remainder at 800ºC. Thus, the iron oxide content was obtained considering that the composite's residual char corresponds to both, residual PU matrix and ferric oxide. The residual mass corresponding to the matrix was subtracted from the residual char of the composite samples and the difference was converted to magnetite mass. The results obtained are presented in Table 1. Obviously, the residual char increased with the concentration of NPs, which confirmed the increased amount of iron oxides present in the material. However, it is also clear that the actual concentration calculated from the TGA results is lower than the nominal one, and the differences between both concentrations become more important as the content of particles increases. The differences can be attributed to the preparation procedure since not all of the NPs included in the film forming suspensions were successfully cast onto the glass plate for drying, i.e. some of the added nanoparticles remained into the flask bottom where the suspension was prepared.

Regarding thermal degradation of the composite samples, from Figure 1 it is clear that none of them lose weight due to adsorbed moisture. However, the differences between the behavior of the neat PU and the derived composites are important: even although two main degradation steps are seen in all curves, the rate of thermal degradation (slope of each zone) is higher for the composites, and the maximum degradation rate takes place at lower

temperature (Tm in Table 1) as particle content increases. In this sense, the maximum decomposition rate for the first degradation step (which involves a weight loss higher than 50%) occurs at 389.9ºC for the neat matrix, and decreased with the addition of NPs until 349.2ºC for the sample with 5 wt.% NPs, then remained approximately constant for the most concentrated samples. These effects could be associated with the increase in thermal conductivity of the material due to the addition of NPs, resulting also in lower temperatures at which the thermal degradation initiates (Ti in Table 1) as particle concentration increases. This degradation step is normally associated with both the dissociation of urethane bonds into isocyanate and alcohol and to the formation of primary or secondary amines, olefin and carbon dioxide [28-30]. The second decomposition step is attributed to the decomposition of the soft segments (polyol backbone) into carbon monoxide, carbon dioxide, carbonyls (aldehyde, acid, acrolein) olefins and alkenes [29-31]. On the other hand, magnetite converts into ferric oxide due to heating, as was reported elsewhere [32]. This process takes place in the range of 130–330 °C, according to the following equation [32, 33]:

$$4Fe_3O_4 + O_2 \rightarrow 6Fe_2O_3$$
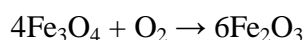
and thus involves a slight increase in the weight of the composite sample due to the absorption of extra oxygen molecules that is over compensated by the weight loss of the PU matrix.

Figure 1

3.3.2. Contact angle

Table 2 presents the results of contact angle measured on the upper and lower film surfaces (surface in contact with air during the drying step and the surface in contact with the glass mold bottom, respectively). The contact angle is one of the basic wetting properties of materials that reveals the hydrophilic/hydrophobic character of the film surface. In this work, the measurements were performed using ethylene glycol, a polar solvent, and thus an increase in the contact angle indicates a density reduction of polar groups on the film surface [19]. It can be seen that there were not significant changes in this property for the PU matrix and composite samples up to 5% NPs nominal concentration, which denotes

homogeneity in the structure of the material. i.e. no accumulation/sedimentation of the nanoparticles on one side of the films, since the angles meassured on both film surfaces are comparable. On the other hand, more concentrated samples (7 wt.% and 10 wt.% NPs) exhibit clear differences on the two surfaces, the lower being less polar than the upper. Due to the differences in the density of the PU matrix ($\sim$1.25 g/cm^3 [1]) and magnetite (5.175 g/cm^3 [35]) and the long time required for drying the films (24 h), some particles can settle on the bottom of the mold, leading to a high density of hydrophilic groups on the lower film surface. Similarly, as the NPs content increases, some particles could agglomerate, favoring the settling.

3.3.3. Differential scanning calorimetry measurements

Figure 2 shows the thermograms of the PU films with and without NPs from -60ºC up to 160ºC, and Table 3 summarizes some of the associated parameters. Three transitions are observed in this temperature range. As expected, the low temperature glass transition (Tg) occurs around -47ºC in all cases and is due to the soft segment phase. Also, the melting temperature and heat of melting of the PU soft segments ($T_{m,s}$ and $\Delta H_{m,s,}$ respectively) decrease slightly with NPs addition. The incorporation of nanoparticles could interfere with the alignment of the chain segments, leading to more imperfect packaging, and thus to crystals that melt at lower temperatures, and also resulting in lower crystallinity. The results depend, not only on the concentration of nanoparticles, but also on their dispersion, since the interface will play an important role in the process. In our case, it is clearly seen that the sample containing 10 nominal wt.% NPs exhibits lower heat of melting, which can be associated with the difficulty of obtaining good nanoparticle dispersion when relative high contents of particles are incorporated into the sample. Furthermore, from the DSC curves, the glass transition associated with the hard segments can barely be observed, as reported in previous works on SPUs [13,36]. It could be located between 90º and 95ºC for all NPs concentration, but the technique sensitivity is not enough to allow accurate calculations. Moreover, the melting of PU hard segments ($T_{m,h}$) appears as smooth peaks varying from 138.2ºC up to 141.7ºC with the addition of NPs. In this case, the addition of NPs increases the hydrogen bond interactions between the urethane groups in hard segments and the oxygen atoms in magnetite, leading to slightly higher melting points. However, the associated heats of melting ($\Delta H_{m,h}$) are very low (with high calculated standard deviations),

indicating that the interactions developed between NPs and polar hard segments do not substantially change the thermal behavior of nanocomposite samples, as compared with that of the neat PU.

Figure 2

3.3.4. Infrared spectroscopy

Figure 3 presents the infrared spectra of the magnetite NPs, neat thermoplastic polyurethane and polyurethane composites. Characteristic peaks (octahedral and tetrahedral Fe-O peaks) of magnetite are observed in the curve corresponding to the NPs at 630 cm^{-1} and 540 cm^{-1}, respectively [37]. Moreover, the bands centered at 3340 cm^{-1} and 1630 cm^{-1} are assigned to O-H vibrations absorbed on the surface of Fe_3O_4 nanoparticles [18]. Regarding PU matrix and composite samples, it is well accepted that the N-H stretching around 3330 cm^{-1}, the C=O vibration at 1725 cm^{-1} and, more recently, the role played by the amide II band at 1524 cm^{-1} and amide III at 1225 cm^{-1} are associated with the hydrogen bond interactions in polyurethanes [38]. The wide band centered at 3330 cm^{-1} corresponds to the hydrogen-bonded N-H stretching vibration present in urethane linkages, and the bands at 1524cm^{-1} correspond to the stretching vibration of C=N group (amide-II band) combined with N-H bending vibration characteristics of the PU structure. Low intensity in the "free" N-H band at 3440 cm^{-1} is observed, which confirms that most of these groups are involved in H-bond interactions among the hard segments [39]. This fact is corroborated by the observation of the C=O stretching vibration around 1726 cm^{-1}, attributed to H-bonded carbonyl groups in disordered ''amorphous'' conformations [40, 41], which appears with a shoulder at 1702 cm^{-1} that corresponds to H-bonded carbonyl groups in ordered ''crystalline'' hard domains [40-42]. Also, the C-H symmetric and asymmetric stretching vibrations of methylene/methyl groups are observed between 2860 cm^{-1} and 2970 cm^{-1}. On the other hand, the broad band of absorption in the range of 490-760 cm^{-1} that corresponds to the Fe-O bonds is only slightly noticeable in the spectrum corresponding to the most concentrated sample, as observed in related papers [21].

Figure 3

3.3.5. X-ray diffraction (XRD)

The X-ray diffraction patterns corresponding to neat NPs, neat PU matrix and PU based composites are presented in Figure 4. The positions and relative intensities of all diffraction peaks found in the pattern of the nanoparticles agree with those of the standard crystal of magnetite (Fe_3O_4) or maghemite (Fe_2O_3) [43-45] and, therefore, the absence of other iron oxides and compounds such as oxidation products is confirmed. In addition, the crystal size of the magnetic particles can be determined using Scherrer's equation [45]:

$$D= \kappa.\lambda/ \beta. \cos (\theta)$$

where: κ= Scherrer Constant (0.9) [38] ; λ= Radiation wavelength (Cu K α =0.1546 nm); β=Width at half height of the selected peak in radians=0.0157; θ=Bragg angle=0.3115. According to this equation, and using the diffraction signal corresponding to the (311) plane of the diffraction pattern of NPs powder, the crystallite size was calculated as 9.3 nm, a value that is closer to the values obtained in previous works [18-22].

Regarding polyurethane based composites, microphase separation or microphase mixing of soft and hard segments depends on their composition and structural order. Therefore, for all composite samples, the broad peaks appearing in the XRD patterns indicate that we are dealing with a low crystalline material [46] of semi-crystalline nature, and implies the formation of a non-ordered structure because of microphase mixing, as was also confirmed by FTIR analysis. According to Hong et al. [47], the diffraction peaks at 2θ = 21.3 and 24.4 are due to the soft segment crystalline phase. The peak intensity is related to the level of crystallinity in the sample [46], therefore it is clear that crystallinity of the soft segment phase decreased as the magnetite concentration in the samples increased, which suggests that the crystallization of the PU matrix is limited somehow by the nanoparticles, as was previously anticipated from the DSC results and was observed in related papers [48, 49]. On the other hand, the peaks corresponding to magnetite nanoparticles appear with increased intensity in the composite patterns as the concentration of filler increases, as expected.

Figure 4

3.3.6. Tensile behavior

A summary of the mechanical properties measured from the tensile tests is presented in Table 4. Surprisingly, the addition of NPs to the PU matrix leads to a decrease in the Young's modulus up to 25% for the most concentrated sample with respect to the value of the neat matrix; while the yield strength decreases up to 21% for the same case. The deformation at break (ε_b) reaches a maximum value of 552% for the film containing 5 wt.% NPs and then decreases. Magnetic NPs are more rigid than PU matrix, thus an increase in the modulus with NPs concentration was the expected behavior. However, particle agglomeration could reduce their effective rigidity. On the other hand, PU crystals also should contribute to augment elastic modulus and, in this work, it was found that that their concentration decreases with magnetite concentration. Probably the combination of those factors, added to reduced compatibility between nanoparticles and polymeric matrix (i.e. particles acting as a defect more than as a reinforcement), would explain the observed behavior.

3.3.7. Dynamical mechanical analysis

Figure 5 shows the dynamic mechanical response of nanocomposites. From Figure 5A it is clear that the addition of nanoparticles to the polymeric matrix does not significantly affect either the absolute value of the storage modulus or its dependence on temperature. For example, nanocomposites containing 3 and 10 wt.% NPs show a slightly higher storage modulus than the neat matrix, while those containing 1 and 7 wt.% present the opposite behavior, but the changes are considered to be within experimental error. Between the storage moduli at -48 °C or lower (glassy region) and 30 °C, the variation is about 50-fold. Moreover, at temperatures slightly higher than 30 °C, samples enter quickly into a kind of flow region and the test should be stopped, which demonstrates the importance of the contribution of the crystalline soft segment phase to the sample stiffness. This variation of modulus is a key point to utilize and control the shape memory effects of a material based on shape memory polyurethanes [15]. Thus, that this change in the storage modulus values before (glassy state) and after the glass transition (rubbery modulus) of the soft segments was maintained in the nanocomposite samples indicates that the "switch temperature" for

the shape-memory properties exhibited by the neat polyurethane was preserved in the PU nanocomposites.

Figure 5

Figure 5B shows that the glass transition temperature of the nanocomposites (arbitrarily taken in this case as the temperature at which the maximum peak in tan δ occurs), is about -36.5ºC ± 0.4 ºC, independently of the NPs concentration. This result is in agreement with the results obtained from DSC curves and with those reported by Mohr and co-workers [23] who incorporate magnetite nanoparticles coated with silica into a polyurethane matrix and did not observe important changes in the glass transition temperature of the composites with respect to that of the neat matrix.

3.3.8. Thermal cyclic tests

Thermal tensile cycling (deformation at high temperature followed by cooling and further recovery at high temperature) was the procedure selected to study the shape memory behavior of unreinforced PU and resulting nanocomposites. The results of the dynamic mechanical tests were used to select these temperatures, and thus they were fixed at 30 ºC (high temperature) and -48 ºC (cooling temperature). Table 5 summarizes the results for all the samples submitted to 100% deformation. In all cases, the first cycle is clearly distinct from the others, with samples showing a relatively low recovery value of about 60%, as has been repeatedly pointed out in the literature [13]. Also, the recovery, calculated with respect to the previous cycle, increased after the second cycle in all the cases. Apparently, the reorientation of the polymer chains of the original cast films that takes place during the first cycle facilitates stretching and relaxation from the second cycle onwards [13]. According to Auad et al. [10], shape recovery is mainly related to hard segment stability: during the first elongation step some weak interactions between the hard segments are damaged and cannot be rebuilt before the next cycle. However, some strong interactions remain and, after the first cycle, the behavior becomes completely reversible, and thus recovery values of about 90% are achieved. On the other hand, Table 5 shows that fixity values are about 97% on average and do not show clear dependence on cycling nor on

particle concentration. As stated elsewhere [13], the controlling factor for fixity is the orientation and molecular stretching reached by the soft segments during elongation. That configuration is essentially frozen after reaching the maximum elongation by lowering the temperature, and the resulting fixity is dependent on the modulus of this non-equilibrium configuration. Evidently, the addition of magnetic nanoparticles to the PU matrix does not modify this behavior. Mosleh et al [49] observed a remarkable drop in shape recovery with nanomagnetite concentration (about 70 % at 5 wt.% nanomagnetite loading, composite samples based on thermoplastic polyurethane segmented block copolymer and poly(ε-caprolactone) (PCL) with a weight ratio of 70/30). They attributed this to particle aggregation in the polymeric matrix as well as to particles being rigid solids that act as obstacles and hinder recovery of the polymer chains. However, in this work, no clear dependence on nanoparticle concentration or percolation thresholds for any property could be observed.

3.3.9. Magnetic nanoparticle heating

All the nanocomposites exhibit magnetic behavior, as was qualitatively corroborated by approaching a magnet to the film samples (as an example, Figure 6 shows the behavior of samples containing 0 and 10 nominal wt.% NPs). Figure 7 shows an image taken with a thermographic camera 15 seconds after turning on an alternating field of 260 kHz and 48 kA/m, when the sample reaches temperatures above 60ºC. The time-temperature curve for the sample in the presence of such a magnetic field was recorded (not shown) and indicates that the temperature within the material surpasses the melting point of PU soft segments in about 10 seconds. Also, the shape memory behavior triggered by alternating-magnetic-field heating was evaluated. Figure 8 shows images of the heating experiment on the PU-10 sample under application of a radiofrequency field, where a fast and almost complete recovery of the original shape of the nanocomposite is reached in about 30 seconds. Thus, the introduction of an indirect triggering method of the shape recovery via magnetic nanoparticle heating is successfully demonstrated.

Figure 6

Figure 7

Figure 8

4. CONCLUSIONS

Magnetic nanocomposites with shape memory properties were prepared by a simple casting procedure. Thermogravimetric analysis of the samples revealed that most of the suspended magnetite NPs could be successfully incorporated into the polyurethane matrix, and thus composite samples with up to 7 wt.% actual concentration were obtained. The thermal degradation of nanocomposite samples and their maximum degradation rate occurred at lower temperatures than that corresponding to the neat PU, which is attributed to the increased thermal conductivity of the material due to the addition of NPs. Contact angle measurements indicated that samples containing up to 5% nominal wt.% are homogenous as regards NPs distribution in the thickness of nanocomposite samples, while the most concentrated exhibit NPs sedimentation/agglomeration of particles at the bottom of the specimens. Even so, differential scanning calorimetry, infrared spectroscopy and X-ray results indicated that the addition of magnetic nanoparticles did not substantially change the microstructure, thermal transitions and crystallinity of the PU matrix. Tensile tests revealed that the modulus and yield strength of the nanocomposites were lower than those of the neat polyurethane for samples containing g 1-5 nominal wt.% NPs, being even more deformable than the neat matrix. The dynamic mechanical behavior of the composites was similar to that of the neat matrix, exhibiting a 50-fold variation between the storage modulus in the glassy and rubbery states. As an expected result, the shape memory behavior, evaluated through tensile cyclic tests, was independent of NP concentration. Finally, all nanocomposite samples exhibited magnetic behavior, and could be heated by applying an alternating magnetic field, leading to quick and almost complete recovery of the previously imposed deformation.

REFERENCES

[1] W.M. Huang, B. Yang, Y.Q. Fu, Polyurethane shape memory polymers, 1st ed., CRC Press, USA, 2011.

[2] J. Leng, X. Lan, Y. Liu, S. Du, Shape-memory polymers and their composites: stimulus methods and applications, Prog. Mater. Sci. 56 (2011) 1077–1135.

[3] M. Behl, M.Y. Razzaq, A. Lendlein, Multifunctional Shape-Memory Polymers, Advanced materials 22(31) (2010) 3388-3410.

[4] D. Ratna, J. Karger-Kocsis, Recent advances in shape memory polymers and composites: a review, J. Mater. Sci. 43 (2008) 254–269.

[5] P.T. Mather, X. Luo, I.A. Rousseau, Shape memory polymer research, Annu. Rev. Mater. Res. 39 (2009) 445–471.

[6] H. Meng, G. Li, A review of stimuli-responsive shape memory polymer composites, Polymer 54 (2013) 2199-2221.

[7] J. Hu, Y. Zhu, H. Huang, J. Lu, Recent advances in shape-memory polymers: Structure, mechanism, functionality, modeling and applications, Progress in Polymer Science 37 (2012) 1720-1763.

[8] M.D. Hager, S. Bode, C. Weber, U.S. Schubert, Shape memory polymers: past, present and future developments, Progress in Polymer Science 49 (2015) 3-33.

[9] H. Tobushi, E. Pieczyska, Y. Ejiri, T. Sakuragi, Thermomechanical properties of shape-memory alloy and polymer and their composites, Mechanics of Advanced Materials and Structures 16(3) (2009) 236-247.

[10] M.L. Auad, V.S. Contos, S. Nutt, M.I. Aranguren, N.E. Marcovich, Characterization of nanocellulose reinforced shape memory polyurethanes, Polymer Int. 57 (2008) 651-659.

[11] I. Yilgör, E. Yilgör, G.L. Wilkes, Critical parameters in designing segmented polyurethanes and their effect on morphology and properties: A comprehensive review, Polymer 58 (2015) A1-A36.

[12] M.L. Auad, M.A. Mosiewicki, T. Richardson, M.I. Aranguren, N.E. Marcovich, Nanocomposites made from cellulose nanocrystals and tailored segmented polyurethanes, Journal of Applied Polymer Science 115(2) (2010) 1215-1225.

[13] M.L. Auad, T. Richardson, M. Hicks, M.A. Mosiewicki, M.I. Aranguren, N.E. Marcovich, Shape memory segmented polyurethanes: dependence of behavior on nanocellulose addition and testing conditions, Polymer International 61(2) (2012) 321-327.

[14] J.W. Cho, Y.C. Jung, Y.C. Chung, B.C. Chun, Improved mechanical properties of shape-memory polyurethane block copolymers through the control of the soft-segment arrangement, Journal of applied polymer science 93(5) (2004) 2410-2415.

[15] M.Y. Razzaq, M. Anhalt, L. Frormann, B. Weidenfeller, Mechanical spectroscopy of magnetite filled polyurethane shape memory polymers, Materials Science and Engineering A 471 (2007) 57–62.

[16] I.A. Rousseau, Challenges of shape memory polymers: A review of the progress toward overcoming SMP's limitations, Polymer Engineering & Science 48(11) (2008) 2075-2089.

[17] R. Hergt, S. Dutz, R. Müller, M. Zeisberger, Magnetic particle hyperthermia: nanoparticle magnetism and materials development for cancer therapy, Journal of Physics: Condensed Matter 18(38) (2006) S2919.

[18] C. Meiorin, D. Muraca, K. Pirota, M.I. Aranguren, M.A. Mosiewicki, Nanocomposites with superparamagnetic behavior based on a vegetable oil and magnetite nanoparticles, European Polymer Journal 53 (2014) 90-99.

[19] G.A. Kloster, N.E. Marcovich, M.A. Mosiewicki, Composite films based on chitosan and nanomagnetite, European Polymer Journal 66 (2015) 386-396.

[20] G.A. Kloster, D. Muraca, C. Meiorin, K.R. Pirota, N.E. Marcovich, M.A. Mosiewicki, Magnetic characterization of chitosan–magnetite nanocomposite films, European Polymer Journal 72 (2015) 202-211.

[21] G.A. Kloster, D. Muraca, M.A. Mosiewicki, N.E. Marcovich, Magnetic composite films based on alginate and nano-iron oxide particles obtained by synthesis "in situ", European Polymer Journal 94 (2017) 43-55.

[22] J. Puig, C.E. Hoppe, L.A. Fasce, C.J. Pérez, Y. Piñeiro-Redondo, M. Bañobre-López, M.A. López-Quintela, J. Rivas, R.J.J. Williams, Superparamagnetic nanocomposites based on the dispersion of oleic acid-stabilized magnetite nanoparticles in a diglycidylether of bisphenol A-based epoxy matrix: magnetic hyperthermia and shape memory, The Journal of Physical Chemistry C 116(24) (2012) 13421-13428.

[23] R. Mohr, K. Kratz, T. Weigel, M. Lucka-Gabor, M. Moneke, A. Lendlein, Initiation of shape-memory effect by inductive heating of magnetic nanoparticles in thermoplastic polymers, Proceedings of the National Academy of Sciences of the United States of America 103(10) (2006) 3540-3545.

[24] P.R. Buckley, G.H. McKinley, T.S. Wilson, W. Small, W.J. Benett, J.P. Bearinger, D. J. Maitland, Inductively heated shape memory polymer for the magnetic actuation of medical devices, IEEE transactions on biomedical engineering 53(10) (2006) 2075-2083.

[25] T. Weigel, R. Mohr, A. Lendlein, Investigation of parameters to achieve temperatures required to initiate the shape-memory effect of magnetic nanocomposites by inductive heating, Smart Materials and Structures 18(2) (2009) 025011.

[26] K. Petcharoen, A. Sirivat, Magneto-electro-responsive material based on magnetite nanoparticles/polyurethane composites, Materials Science and Engineering: C 61 (2016) 312-323.

[27] R. Massart, V. Cabuil, Synthèse en milieu alcalin de magnétite colloïdale: contrôle du rendement et de la taille des particules = Synthesis of colloidal magnetite in alkaline medium: yield and particle size control, Journal de chimie physique 84(7-8) (1987) 967-973.

[28] I. Javni, Z.S. Petrović, A. Guo, R. Fuller, Thermal stability of polyurethanes based on vegetable oils, Journal of Applied Polymer Science 77(8) (2000) 1723-1734.

[29] L. Shufen, J. Zhi, Y. Kaijun, Y. Shuqin, W.K. Chow, Studies on the thermal behavior of polyurethanes, Polymer-plastics technology and engineering 45(1) (2006) 95-108.

[30] P.K. Pillai, S. Li, L. Bouzidi, S.S. Narine, Metathesized palm oil polyol for the preparation of improved bio-based rigid and flexible polyurethane foams, Industrial Crops and Products 83 (2016) 568-576.

[31] S. Gryglewicz, W. Piechocki, G. Gryglewicz, Preparation of polyol esters based on vegetable and animal fats, Bioresource Technology 87(1) (2003) 35-39.

[32] K. Cendrowski, P. Sikora, B. Zielinska, E. Horszczaruk, E. Mijowska, Chemical and thermal stability of core-shelled magnetite nanoparticles and solid silica, Applied Surface Science 407 (2017) 391–397.

[33] E.R. Monazam, R.W. Breault, R. Siriwardane, Kinetics of magnetite (Fe_3O_4) oxidation to hematite (Fe_2O_3) in air for chemical looping combustion, Ind. Eng. Chem. Res. 53 (34) (2014) 13320–13328.

[34] Z.S. Petrovic, I. Javni, V. Divjakovic, Structure and physical properties of segmented polyurethane elastomers containing chemical crosslinks in the hard segment, Journal of Polymer Science Part B Polymer Physics 36(2) (1998) 221-235.

[35] J.W. Anthony, R.A. Bideaux, W.B. Kenneth, C.N. Monte, Eds., Handbook of Mineralogy, Mineralogical Society of America, Chantilly, VA 20151-1110, USA. http://www.handbookofmineralogy.org/.

[36] B.C. Chun, T.K. Cho, Y.C. Chung, Blocking of soft segments with different chain lengths and its impact on the shape memory property of polyurethane copolymer, Journal of Applied Polymer Science 103(3) (2007) 1435-1441.

[37] G.G. Utkan, F. Sayar, P. Batat, S. Ide, M. Kriechbaum, E. Pişkin, Synthesis and characterization of nanomagnetite particles and their polymer coated forms, Journal of colloid and interface science 353(2) (2011) 372-379.

[38] C. Zhang, Z. Ren, Z. Yin, H. Qian, D. Ma, Amide II and amide III bands in polyurethane model soft and hard segments, Polymer Bulletin 60(1) (2008) 97-101.

[39] L. Zha, M. Wu, J. Yang, Hydrogen bonding and morphological structure of segmented polyurethanes based on hydroquinone–bis (β-hydroxyethy) ether as a chain extender, Journal of Applied Polymer Science 73(14) (1999) 2895-2902.

[40] A. Eceiza, M.D. Martin, K. De la Caba, G. Kortaberria, N. Gabilondo, M.A. Corcuera, I. Mondragon, Thermoplastic polyurethane elastomers based on polycarbonate diols with different soft segment molecular weight and chemical structure: mechanical and thermal properties, Polymer Engineering & Science 48(2) (2008) 297-306.

[41] I. Yilgör, E. Yilgör, I.G. Guler, T.C. Ward, G.L. Wilkes, FTIR investigation of the influence of diisocyanate symmetry on the morphology development in model segmented polyurethanes, Polymer 47 (2006) 4105–4114.

[42] M.M. Coleman, D.J. Skrovanek, J. Hu, P.C. Painter, Hydrogen bonding in polymer blends. 1. FTIR studies of urethane-ether blends, Macromolecules 21(1) (1988) 59-65.

[43] A.S. Bhatt, K.D. Bhat, M.S. Santosh, Electrical and magnetic properties of chitosan–magnetite nanocomposites, Physica B: Condensed Matter 405(8) (2010) 2078–2082.

[44] L. Zhang, X. Zhu, H. Sun, G. Chi, J. Xu, Y. Sun, Control synthesis of magnetic Fe_3O_4-chitosan nanoparticles under UV irradiation in aqueous system, Curr. Appl Phys. 10 (2010) 828–833.

[45] J. Chen, P. Yang, Y. Ma, T. Wu, Characterization of chitosan magnetic nanoparticles for in situ delivery of tissue plasminogen activator, Carbohydr. Polym. 84 (2011) 364–372

[46] M. Shahrousvand , M.S. Hoseinian, M. Ghollasi, A. Karbalaeimahdi, A. Salimi, F.A. Tabar, Flexible magnetic polyurethane/Fe_2O_3 nanoparticles as organic-inorganic nanocomposites for biomedical applications: Properties and cell behavior, Materials Science and Engineering: C 74 (2017) 556-567.

[47] J.H. Hong, H.J. Jeon, J.H. Yoo, W.R. Yu, J.H. Youk, Synthesis and characterization of biodegradable poly (3-caprolactone-co-b-butyrolactone)-based polyurethane, Polymer Degradation and Stability 92 (2007) 1186-1192

[48] H. Qiao-ling, W.U. Jia, C. Fu-ping, S. Jia-cong, Biomimetic preparation of magnetite/chitosan nanocomposite via in situ composite method-Potential use in magnetic tissue repair domain, Chem. Res. Chinese U. 22(6) (2006) 792-796.

[49] Y. Mosleh, N.G. Ebrahimi, A. Mahdavian, M. Ashjari, TPU/PCL/nanomagnetite ternary shape memory composites: studies on their thermal, dynamic-mechanical, rheological and electrical properties, Iran Polym. J. 23 (2014) 137–145.

TABLES

Table 1: Thermogravimetric behavior of nanocomposite films.

NPs, nominal content, wt.%	NPs calculated content, wt.%	Ti, ºC	Tm, ºC
0	--	319 ± 14	390 ± 9
1	0.9 ± 0.1	321 ± 6	383 ± 5
3	2.5 ± 0.2	314 ± 6	358 ± 19
5	3.9 ± 0.8	306 ± 8	349 ± 11
7	5.7 ± 1.4	307 ± 5	352 ± 12
10	7.1 ± 0.4	299 ± 9	352 ± 7

Table 2: Contact angle of nanocomposite films.

NPs, nominal wt.%	Contact angle in Lower surface (°)	Contact angle in Upper surface (°)
0	49.8 ± 1.3	46.9 ± 2.8
1	44.9 ± 3.4	69.8 ± 2.9
3	51.3 ± 1.7	53.4 ± 2.1
5	49.1 ± 2.5	49.2 ± 1.9
7	52.7 ± 2.8	66.9 ± 4.1
10	50.4 ± 4.2	62.8 ± 2.2

Table 3: DSC characterization as a function of NPs content

NPs, nominal wt.%	T_g (°C)	$T_{m,s}$ (°C)	$\Delta H_{m,s}$ (J/g*)	$T_{m,h}$ (°C)	$\Delta H_{m,h}$ (J/g*)
0	-46.5 ± 1.1	38.8 ± 0.6	17.1 ± 0.6	138.2 ± 1.8	1.9 ± 0.6
1	-47.8 ± 0.7	37.9 ± 0.8	17.1 ± 0.4	138.0 ± 0.9	2.0 ± 0.4
3	-48.3 ± 0.6	36.8 ± 0.7	17.8 ± 3.1	139.0 ± 3.6	1.3 ± 0.1
5	-47.4 ± 0.1	38.0 ± 0.8	16.5 ± 0.4	140.0 ± 2.5	1.8 ± 1.2
7	-47.4 ± 0.1	37.7 ± 0.1	16.9 ± 0.1	141.6 ± 0.5	1.3 ± 0.3
10	-47.4 ± 0.6	36.7 ± 0.2	15.6 ± 0.1	141.7 ± 2.3	0.9 ± 0.5

* calculated per mass of neat PU

Table 4. Tensile properties of PU-NPs composites.

NPs, nominal wt.%	E (MPa)	Yield stress, σ_y (MPa)	Elongation at break, ε_b (%)
0	2.4 ± 0.1	5.7 ± 0.1	464 ± 31
1	2.4 ± 0.5	5.2 ± 0.3	530 ± 6
3	1.9 ± 0.1	4.7 ± 0.1	550 ± 30
5	2.1 ± 0.1	4.9 ± 0.3	552 ± 26
7	2.0 ± 0.5	4.4 ± 0.2	392 ± 41
10	1.8 ± 0.1	4.5 ± 0.2	394 ± 44

Table 5: Shape memory behavior of shape memory PU composites.

NPs, nominal wt.%	Cycle	ε_u (%)	ε_p (%)	R_f (%)	R_r (%)
PU matrix	1	97.8	36.7	97.8	63.3
0	2	96.9	45.1	96.9	86.6
	3	96.5	47.1	96.5	96.3
PU-1	1	97.8	36.2	97.8	63.9
1	2	97.0	42.6	97.0	89.9
	3	96.7	46.7	96.7	92.8
PU-3	1	96.8	39.0	96.8	61.0
3	2	94.7	44.8	94.7	90.7
	3	95.3	47.6	95.3	94.9
PU-5	1	97.6	40.7	97.6	59.3
5	2	96.5	46.3	96.5	90.0
	3	96.1	47.3	96.1	98.8
PU-7	1	98.0	43.2	97.6	56.8
7	2	97.2	49.0	97.2	89.8
	3	96.8	51.7	96.8	94.7
PU-10	1	97.9	36.7	97.9	63.3
10	2	98.0	41.9	98.0	91.8
	3	98.1	45.8	98.1	93.3

FIGURE CAPTIONS

Figure 1: TGA curves of nanocomposite films.

Figure 2: DSC thermograms of the nanocomposite films. Numbers next to the acronym PU indicate the nominal content of NPs in each sample.

**Figure 3:** FTIR spectra of neat NPs, neat PU matrix and PU based nanocomposites.

Figure 4: X-ray diffraction patterns corresponding to neat NPs, neat PU matrix and PU based composites

Figure 5: Dynamic mechanical response of neat PU matrix and PU-NPs composites. A) Storage shear modulus vs. temperature; B) tan δ vs. temperature.

Figure 6. Magnetic character of the nanocomposite with 10 nominal wt.% NPs (black sample). Neat PU sample (white one) do not show magnetic response.
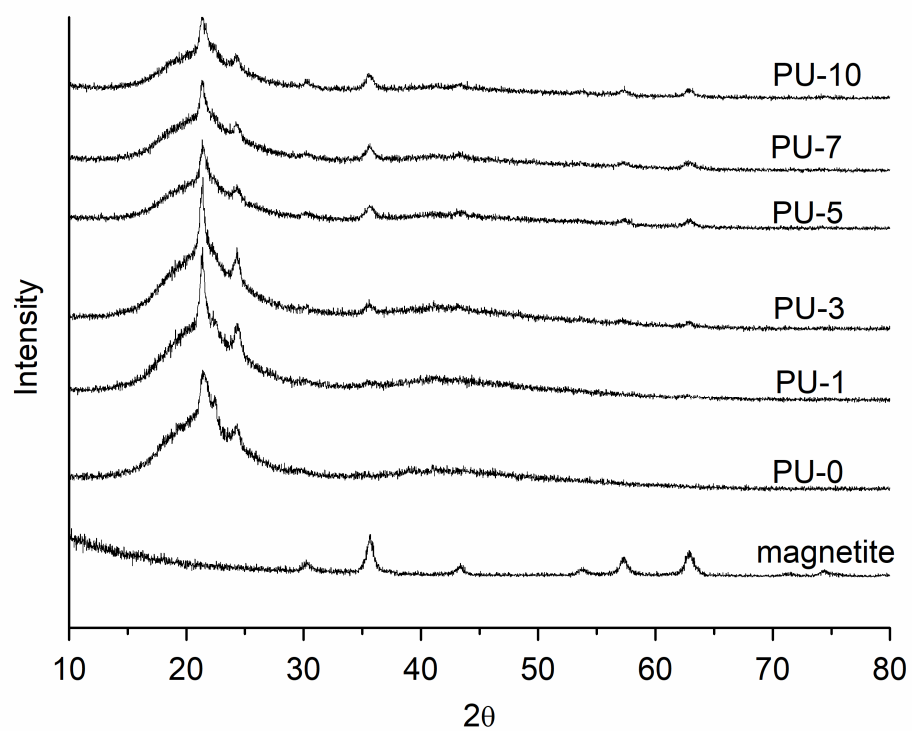
Figure 7. Temperature map for a piece of 4.9 mm x 10.9 mm length of the sample with 10 nominal wt.% of NPs after 15 seconds of application of an alternating magnetic field of 260kHz and 48 kA/m.
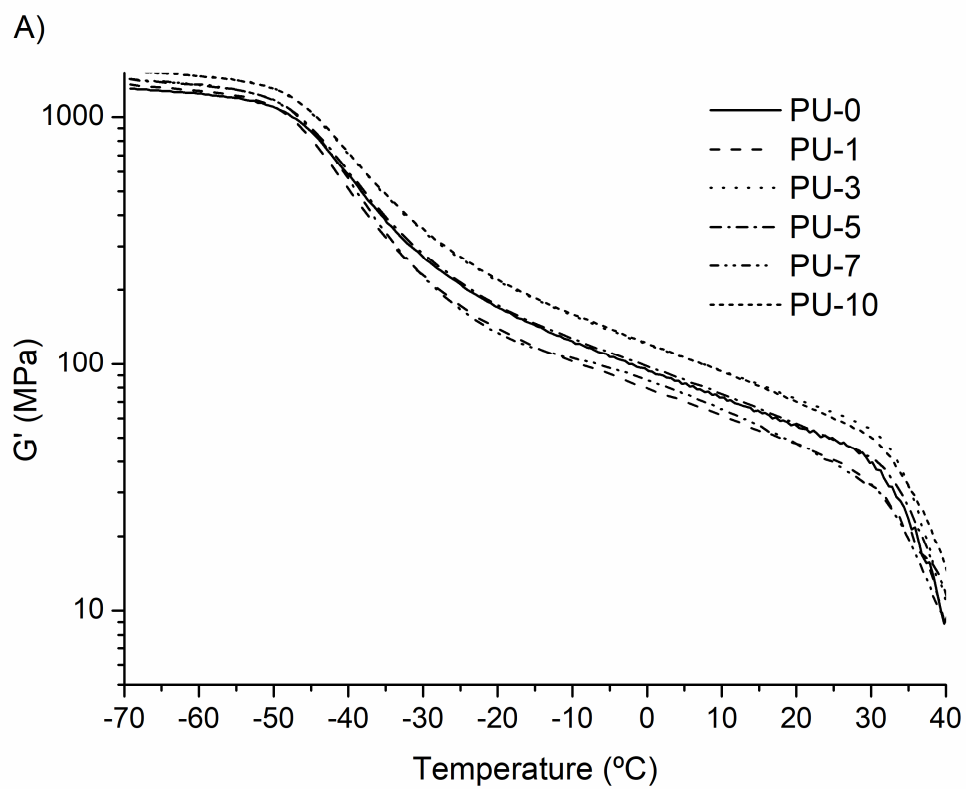
Figure 8. Shape recovery of the sample with 10 nominal wt.% of NPs activated by the application of an alternant magnetic field.
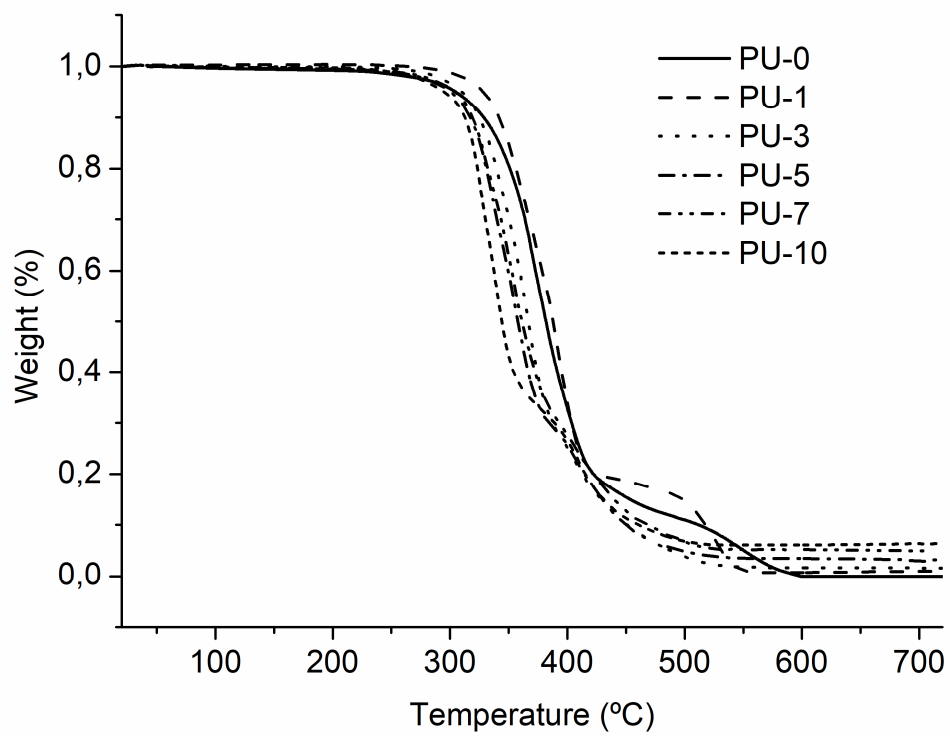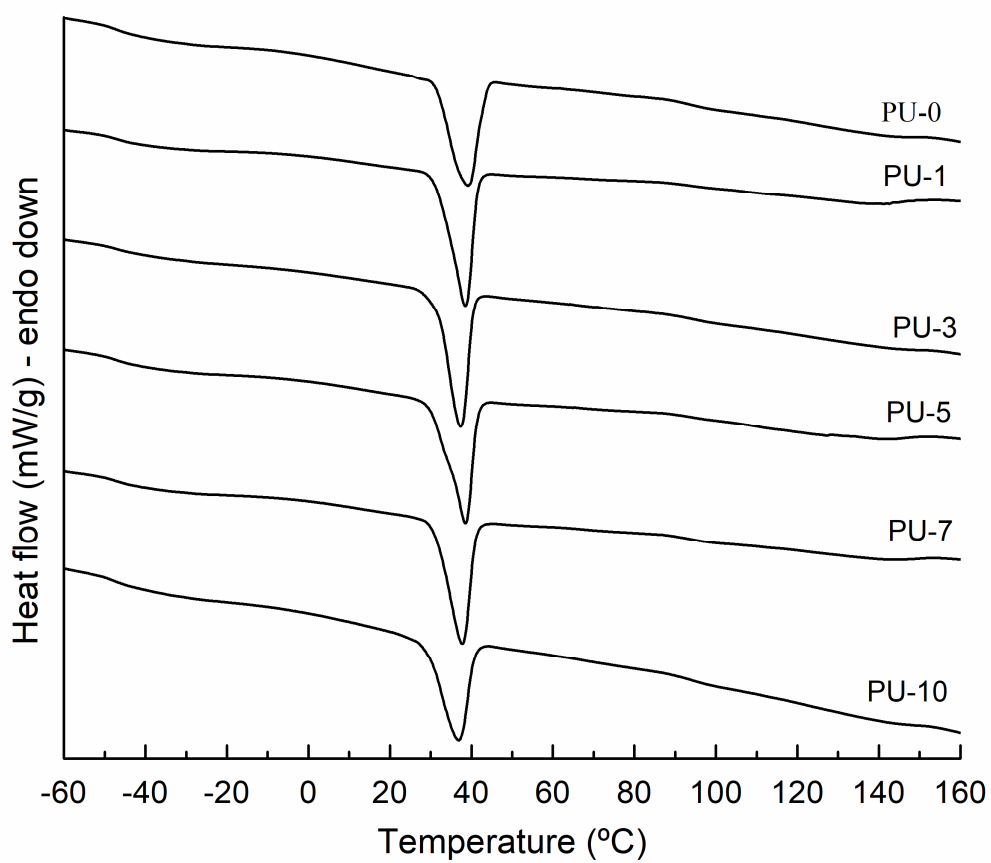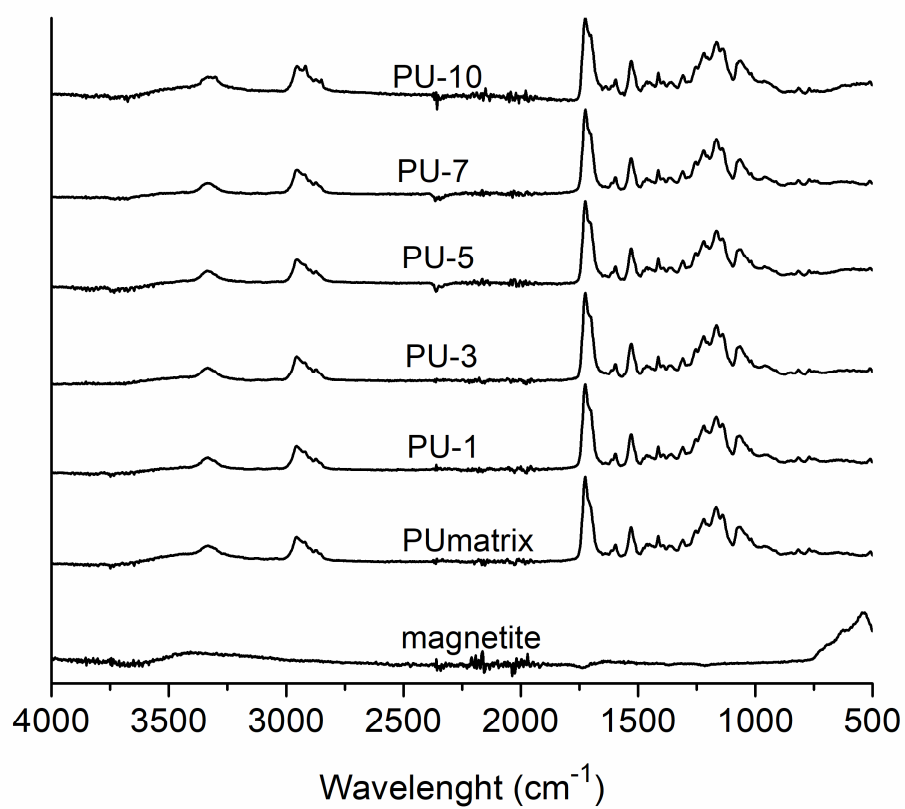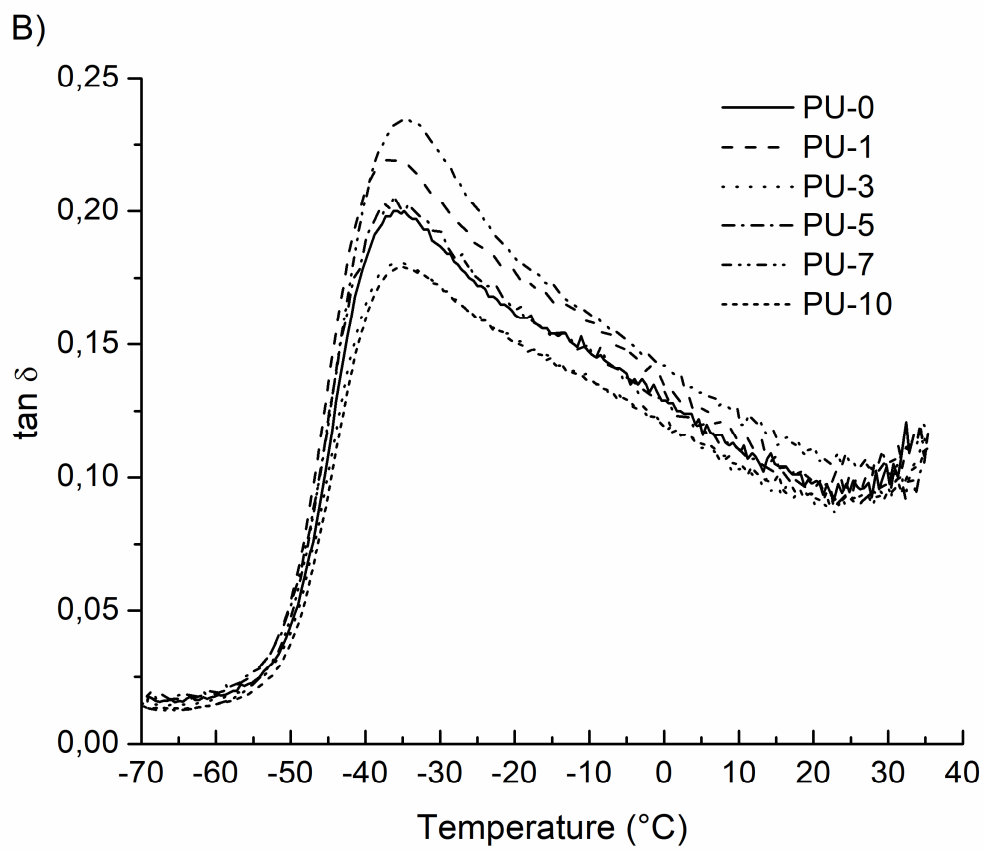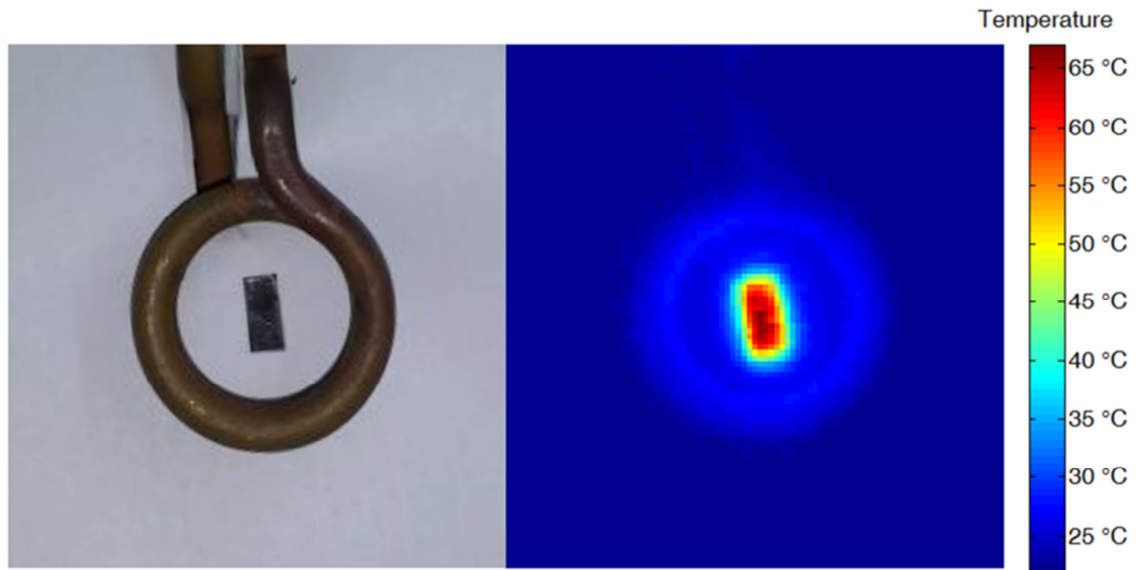
A)

B)

- Magnetic nanocomposites with shape memory properties were prepared by a simple casting procedure.

- Most of the suspended magnetite nanoparticles were successfully incorporated into the polyurethane matrix.

- The addition of magnetic nanoparticles did not change substantially the microstructure, thermal transitions and crystallinity of the polyurethane matrix.

- The shape memory behavior, evaluated through tensile cyclic tests, resulted independent of nanoparticle concentration.

- The original shape was successfully recovered by applying an indirect triggering method via magnetic nanoparticle heating.